Mass-Profile and Instability-Growth Measurements for 300-Wire *Z*-Pinch Implosions Driven by 14–18 MA

D. B. Sinars,* M. E. Cuneo, E. P. Yu, D. E. Bliss, T. J. Nash, J. L. Porter, C. Deeney, M. G. Mazarakis, G. S. Sarkisov, and D. F. Wenger

Sandia National Laboratories, P.O. Box 5800, Albuquerque, New Mexico 87185-1193, USA
(Received 30 April 2004; published 28 September 2004)

We present the first comprehensive study of high wire-number, wire-array *Z*-pinch dynamics at 14–18 MA using x-ray backlighting and optical shadowgraphy diagnostics. The cylindrical arrays retain slowly expanding, dense wire cores at the initial position up to 60% of the total implosion time. Azimuthally correlated instabilities at the array edge appear during this stage which continue to grow in amplitude and wavelength after the start of bulk motion, resulting in measurable trailing mass that does not arrive on axis before peak x-ray emission.

DOI: 10.1103/PhysRevLett.93.145002 PACS numbers: 52.59.Qy, 52.58.Lq, 52.70.La, 52.80.Qj

High wire-number tungsten wire arrays on the Sandia *Z* facility, a 20 MA, 100 ns pulsed power driver, have produced x-ray powers in excess of 200 TW and total x-ray yields up to 1.8 MJ [1]. *Z* pinches are well known as efficient energy convertors (>10% conversion efficiency from wall plug to soft x rays) [2], but historically the long time scale of the x-ray emission (>10 ns) limited their peak radiation power. Experiments during the last decade increased the peak radiation power by increasing the wire number from ~16 wires to >100 wires [3,4], which shortened the duration of the x-ray emission without affecting the yield. Today, *Z*-pinch x-ray sources are being used as drivers for inertial confinement fusion, complex hydrodynamics, and radiation transport experiments.

Initially it was argued that the dynamics changed as the wire number increased from a collection of individual wire plasma implosions to an implosion of a more azimuthally symmetric plasma shell, assuming that the wires ablate and merge on a time scale short compared to the implosion time [3,4]. An annular shell implosion is dominated by the two-dimensional magneto-Rayleigh-Taylor (MRT) instability [5,6]. This picture was subsequently clouded by single- or few-wire experiments, in which wire explosions driven by 10^{10}–10^{11} A/s, 1–50 kA current pulses were characterized by slowly expanding, dense (~1%–10% solid density) wire cores surrounded by more tenuous "coronal" plasma [7,8]. Wire-array experiments at the 1 MA, 250 ns MAGPIE facility [9,10] and the 3 MA, 100 ns Angara-5-1 facility [11] also observed a complex core/corona structure for extended periods, along with substantially different wire-array dynamics than for annular shell implosions.

The scaling of *Z*-pinch dynamics from 1–3 MA experiments using 16–64 wires to high wire-number, 18 MA experiments is poorly understood. Persistent wirelike features were noted on the 8 MA SATURN facility [12]. Other dynamical features observed at 1–3 MA have been noted on the *Z* facility, such as the early arrival of plasma on axis (from stationary ablating wire cores), a delayed onset of the array implosion, and the inferred presence of substantial mass trailing the main implosion [13]. With the exception of a single optical streak image, however, direct observations were limited to low resolution (~100 μm), chordally or axially integrated self-emission diagnostics. Using radiography diagnostics we have measured for the first time the array mass distribution, including its core/corona structure and the growth and evolution of instabilities, for high wire-number, 14–18 MA wire-array *Z*-pinch implosions. These diagnostics have observed azimuthally correlated instabilities during the core/corona stage for the first time. These grow in a complex, three-dimensional manner and create a distributed implosion with trailing mass that does not arrive on axis until after the peak radiation power occurs. The tests discussed here studied 20 mm diameter, 300-wire arrays. The wire array and x-ray backlighting hardware are described in Fig. 1.

Monochromatic x-ray backlighting instruments at 1.865 and 6.151 keV [14] were the principal diagnostics for these experiments. The x-ray sources for radiography were created using the *Z*-beamlet laser to illuminate Si (or Mn) targets with a ~1 TW pulse of 527 nm light focused to a ~200 μm diameter focal spot for 0.6 ns (1.0 ns for Mn). These backlighters have 9–10 μm spatial resolution in the focal plane of a 4 mm by 20 mm field of view imaged at a magnification of six. The spectral bandpass of these instruments is <0.5 eV, an essential property that allows backlighting in the 1–2 MJ x-ray "background" produced by the wire-array *Z* pinch itself. One backlit image per *Z* facility test was captured on Kodak RAR 2497 (or Kodak DEF) x-ray film. The time-integrated *Z*-pinch self-emission in the same spectral band was also imaged on the film. A 30 mJ, 532 nm Nd:YAG laser was used for the optical shadowgraphy measurements. The ~20 μs beam from the laser was split into six beams

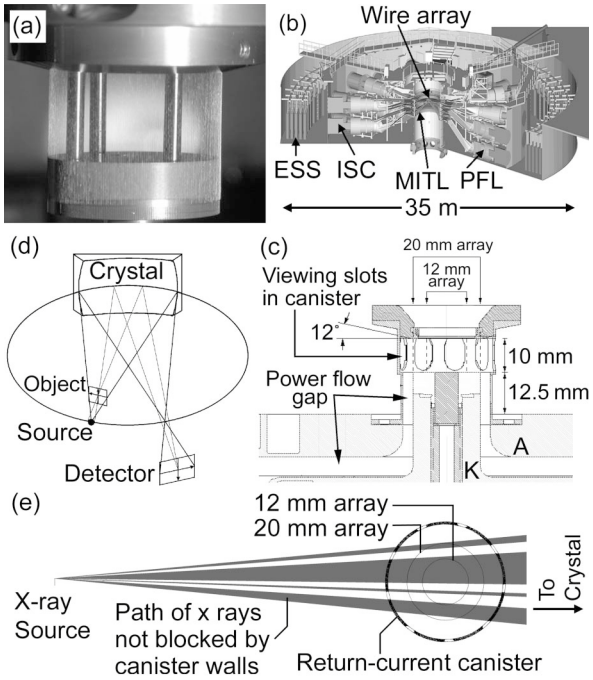

FIG. 1. (a) Photograph of a 20 mm diameter, 300-wire array before installation. (b) Diagram of the Z facility, showing the energy storage section, intermediate storage capacitors, pulse forming lines, and magnetically insulated transmission lines used to deliver current to the wire array. (c) Vertical slice through the load region hardware. The array is surrounded by a return-current canister with nine slots in the horizontal plane for diagnostic access. (d) Conceptual diagram of the spherical crystal x-ray backlighting diagnostic. The crystal acts as an x-ray mirror with a ≤ 0.5 eV spectral bandpass. The detector is placed at the focal point of the object (the array center in these tests). (e) A horizontal slice through the center of the array showing the field of view of the arrays allowed by the return-current canister slots.

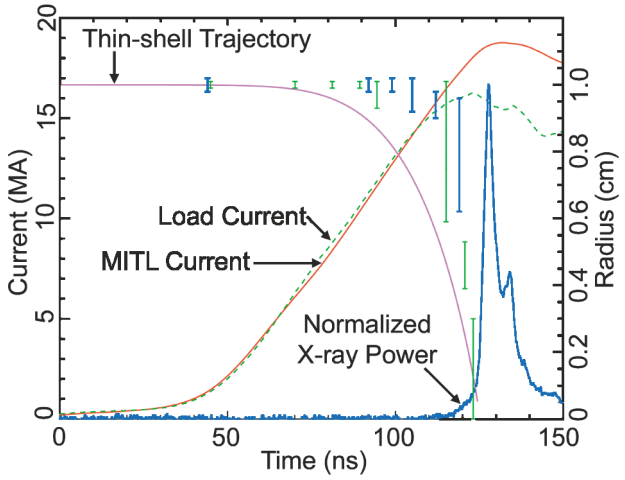

FIG. 2 (color). Data for 20 mm diameter tungsten wire arrays with 300 7.4 μm W wires. The machine and load currents are plotted as red and green curves, respectively, along with the normalized x-ray power from a typical test (z1049), shown in blue. The trajectory for a thin shell with the same total mass (2.5 mg) is overlaid. Also plotted are bars corresponding to the radially outermost and innermost positions of the outer edge of the imploding mass as seen via radiography (green) and optical shadowgraphy (blue).

sent to independent 1.0 ns gated charge-coupled device cameras, allowing six images to be obtained on each test.

In Fig. 2 we plot current and x-ray pulse shapes obtained for one of the arrays studied in these tests. The trajectory of an infinitely thin shell with the same mass, as calculated from Ref. [6], is also plotted. Data obtained during radiography and shadowgraphy tests with this array are also plotted. Some radiography data from Fig. 2 are shown in Fig. 3. The data in Fig. 2 are plotted as ranges, with the top and bottom corresponding to the radially outermost and innermost points of the mass edge visible in the image (e.g., for Fig. 3(e) the range would be 10.0 to 9.2 mm). The radiographs show that the array retains long-lived dense cores that disappear between 81 and 89 ns. The boundaries of the dense cores expand slowly during this time (based on other portions of the image not shown in Fig. 3) until the cores are no longer discernible and the plasma appears to form a shell [Fig. 3(d)]. Even before the cores disappear, an azimuthally correlated axial instability can be seen developing as early as Fig. 3(b) (because of the high wire number, the instabilities seen at the edge include contributions from at least 7–8 wires). The period of this instability appears to be about the same as the wire core diameters at the time of each image (about 50 and 65 μm in Figs. 3(b) and 3(c), respectively). This axial instability was seen in a variety of arrays, examples of which are shown in Fig. 3. Though the axial wavelengths seen in Fig. 3 vary, they are all within 20% of the wire core diameters estimated from other parts of the image (e.g., the period in the Al test is larger than the W test, but so are the Al wire cores.)

Low wire-number array experiments have noted that axial instabilities on individual wires are associated with axially nonuniform mass ablation from its dense core so that the core burns through sooner at some axial positions than others [10]. In our high wire-number case the axially nonuniform ablation becomes azimuthally correlated, so that entire array segments begin imploding before others as seen in Fig. 3(e). The lack of simultaneity in the start of the implosion as a function of axial height creates a broad radial mass distribution immediately. This is in contrast to traditional 2D-MRT calculations (most of which are underresolved with ~ 100 μm zoning) in which initially thin radial mass distributions do not broaden significantly until the mass travels a large fraction of the distance to the axis (see Ref. [6] and references therein). Some portions of the dense cores are left at or near their initial positions after the bulk of the mass has moved in, as seen in the full z1050 radiograph shown in Fig. 4. These pieces dissipate slowly, presumably because most of the current

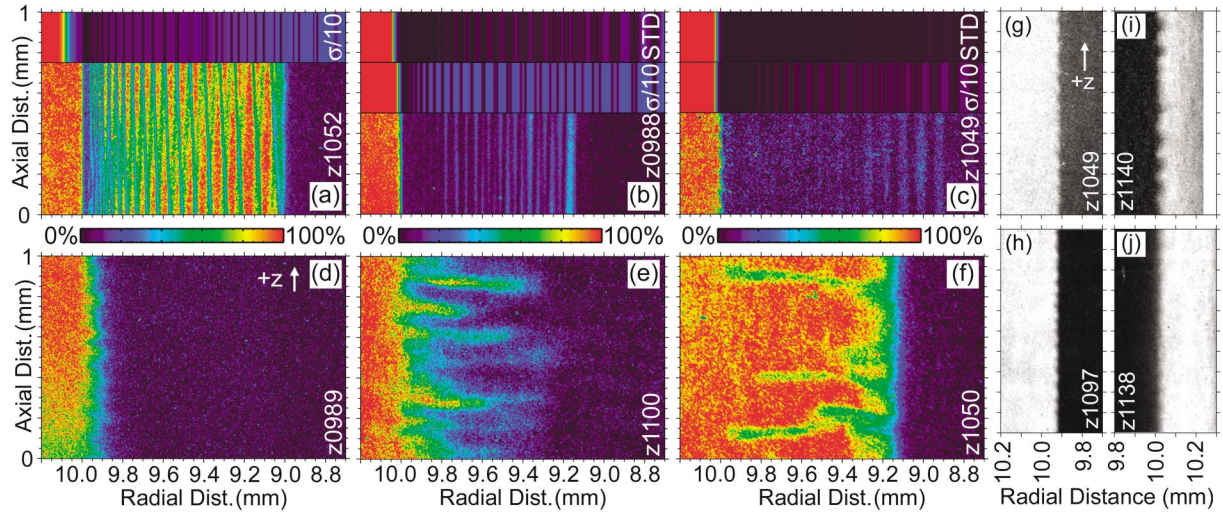

FIG. 3 (color). (a)–(f) Expanded 1.865 keV radiographs showing portions of the edge of 2.5 mg arrays at 45, 70, 81, 89, 95, and 115 ns, respectively. Parts (a)–(c) include artificial radiographs of baseline (STD) and modified ($\sigma/10$) ALEGRA simulations at those times. The modified simulations artificially reduced the electrical conductivities in the cores by a factor of 10 as a method for reducing the wire mass ablation rate as discussed in the text. Axial perturbations, faintly visible as early as frame (b), develop and begin to correlate azimuthally while the array is "wirelike" and seed instability growth later, resulting in trailing mass as in (f). The color scale shown is linear in units of transmission. The arrays in (a) and (b) were slightly twisted. (g)–(j) 1.865 keV radiographs from assorted 20 mm diameter, 300-wire arrays, all taken when the load current was 8.5–8.8 MA. Initial wires were (g) 7.4 μm W, (h) 11.5 μm W, (i) 36 μm Al, and (j) 20 μm Cu. In each case the vertical wavelength was within 20% of the wire core diameter at the time of the image [cores nearly merged in (i)]. A linear black-to-white (0%–100%) scale with transmission was used.

has also already moved inward. About 1%–2% of the total array mass is estimated to reside in the "fingers" seen in Fig. 3(f) between 9 and 10 mm. Optical shadowgraphy images at this time indicate the volume between the fingers includes some plasma that could comprise another few percent of the total mass, based on crude estimates for the sensitivity of that diagnostic ($\sim 10^{18} e/\mathrm{cm}^3$). By the time of the z1054 radiograph in Fig. 4, the mass density inside $r = 9$–10 mm has decreased below the detection limit of the 1.865 keV backlighter. When the low-density plasma observed using shadowgraphy begins to clear out as in Fig. 5, the instabilities resemble MRT calculations in that the instabilities cascade to larger wavelengths. Estimating the acceleration from the images, we infer that the dominant wavelengths in each frame of Fig. 5 [(b)–(e)] grew 7–8 e folds.

The observation of the start of azimuthal correlations prior to the formation of a shell and the clearing out of mass at $r > 5$ mm before the time of peak x rays is different from the 1–3 MA experiments cited earlier, which appear to have a larger fraction of trailing mass. Nonetheless, some trailing mass is still arriving on axis during and after the peak x rays in our tests (see also Ref. [13]). This is illustrated in Fig. 6. The radiograph (taken when the pinch was emitting 20 TW of x rays) shows a highly nonuniform pinch, with substantial mass out to about 3 mm at some axial heights. The x-ray streak camera image from the same test shows the axially averaged radius of the self-emission, with the brightest emission occurring just before the minimum radius of the emission is achieved and just after the peak in the radiation power.

To illustrate the usefulness of these measurements, in Fig. 3 we show artificial radiographs of ALEGRA-HEDP

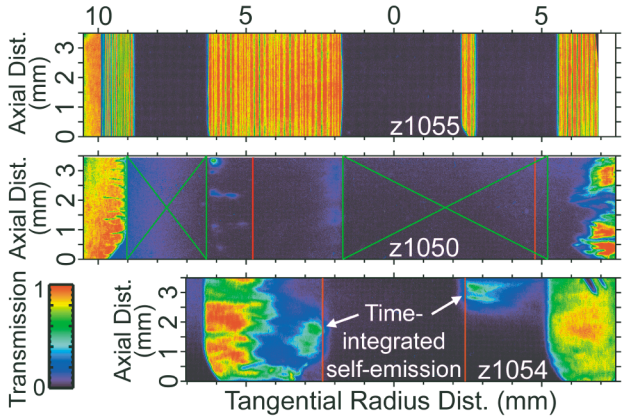

FIG. 4 (color). 1.865 keV radiographs of the 2.5 mg array from Fig. 2. (Top) pretest radiograph from test z1055 illustrating the field of view. (Middle) complete radiograph image test z1050 showing the outer edge of the imploding mass in addition to the expanded region shown in Fig. 3(f). (Bottom) radiograph from test z1054 taken at 121 ns illustrating the highly unstable trailing mass. In the z1050 and z1054 radiographs, the image regions blocked by slots are marked in green and the position of a 0D thin shell at each time is marked in red.

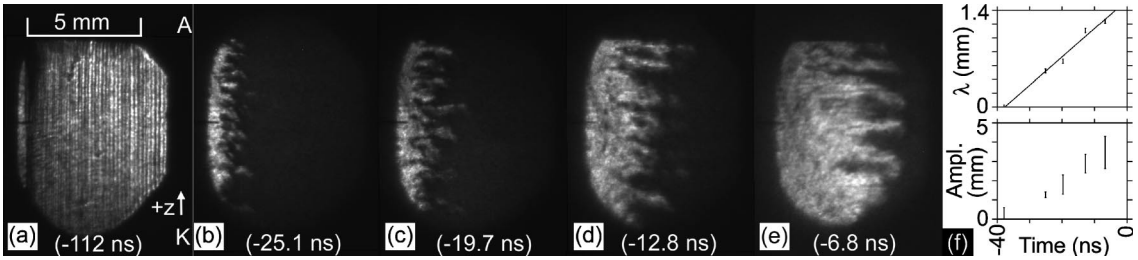

FIG. 5. (a)–(e) Sequence of optical shadowgraphy images from a 20 mm diameter, 300 11.5 μm W wire-array test (z1176) illustrating the growth of instabilities in the low-density trailing mass. (f) Plots of the vertical wavelength and horizontal perturbation amplitudes for five of the six frames from this test. All times shown are relative to peak x rays. Other tests show that this view is empty at the time of peak x rays.

r-θ magnetohydrodynamic simulations at early times. Calculations with the best available radiation, conductivity, and equation of state models couple too much current into the dense cores, causing them to expand and vaporize too rapidly [for example, the cores are completely gone in Fig. 3(c)]. By dividing the electrical conductivity in the cores by factors of 10–100 we can artificially force the simulations to couple less current into the dense cores and thereby obtain longer-lived cores. A thorough discussion of the simulations is beyond the scope of this Letter (some details are discussed in Ref. [13]), and we include them here mainly to emphasize that for the first time a high-quality data set exists for high-current, high wire-number arrays that can be used to benchmark calculations. Ultimately, accurate simulations of the development and growth of azimuthally correlated instabilities while "corelike" structures exist will require three-dimensional simulations. Some initial 3D simulations have been attempted thus far that successfully generate trailing mass with late on-axis arrival [15]. Such calculations are just beginning and a 3D simulation of the full array with the spatial resolution of the experimental data presented here is unfeasible at present.

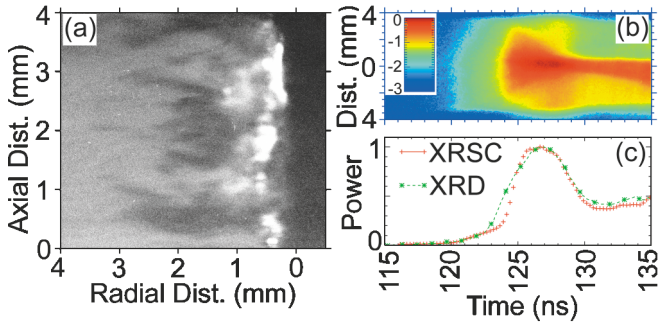

FIG. 6 (color). (a) 6.151 keV radiograph at 123 ns. The white spots are from time-integrated self-emission at 6.151 keV. (b) Streaked self-emission (400–450 eV) from the same test showing the spatial distribution of the self-emission. (c) Spatially integrated line out of the x-ray streak camera (XRSC) data plotted alongside a comparable x-ray diode (XRD) signal.

We thank Dr. J. P. Chittenden, Dr. S.V. Lebedev, and Dr. S. N. Bland of Imperial College, London, for useful discussions on wire-array dynamics. We thank D. Johnson, K. Keller, P. Rambo, S. Rogowski, C. S. Speas, I. Smith, and B. Thurston for their support with diagnostics on Z and Dr. B. M. Jones and Dr. C. Coverdale for additional backlighting test opportunities on Z. We also thank the ALEGRA team, T. Brunner, K. Cochrane, T. Haill, C. Garasi, and A. Robinson. Sandia is a multiprogram laboratory operated by Sandia Corporation, a Lockheed Martin Company, for the National Nuclear Security Administration under DE-AC04-94AL85000.

*Electronic address: dbsinar@sandia.gov

[1] R. B. Spielman *et al.*, Phys. Plasmas **5**, 2105 (1998).
[2] N. R. Pereira and J. Davis, J. Appl. Phys. **64**, R1 (1988).
[3] C. Deeney *et al.*, Phys. Rev. E **56**, 5945 (1997).
[4] T.W. L. Sanford *et al.*, Phys. Rev. Lett. **77**, 5063 (1996).
[5] E. G. Harris, Phys. Fluids **5**, 1057 (1962).
[6] D. D. Ryutov, M. S. Derzon, and M. K. Matzen, Rev. Mod. Phys. **72**, 167 (2000).
[7] S. A. Pikuz *et al.*, Phys. Rev. Lett. **83**, 4313 (1999).
[8] F. N. Beg *et al.*, Plasma Phys. Controlled Fusion **39**, 1 (1997).
[9] S.V. Lebedev *et al.*, Phys. Rev. Lett. **85**, 98 (2000).
[10] S.V. Lebedev *et al.*, Phys. Plasmas **8**, 3734 (2001).
[11] V.V. Alexsandrov *et al.*, Plasma Phys. Rep. **27**, 89 (2001).
[12] C. Deeney *et al.*, Rev. Sci. Instrum. **68**, 653 (1997).
[13] M. E. Cuneo *et al.*, "Characteristics and Scaling of Tungsten Wire Array Z-Pinch Implosion Dynamics at 20 MA" (to be published).
[14] D. B. Sinars *et al.*, Rev. Sci. Instrum. **74**, 2202 (2003).
[15] J. P. Chittenden *et al.*, in *Dense Z-Pinches: 5th International Conference on Dense Z-Pinches, 2002, Albuquerque, NM, USA*, edited by Jack Davis, Christopher Deeney, and Nino R. Pereira, AIP Conf. Proc. No. 651 (AIP, New York, 2002), pp. 354–357.